Combining Intranuclear-Cascade and Preequilibrium Hauser-Feshbach Models for Nuclear Cross-Section Calculations Between 1 MeV and 5 GeV

C. Y. FU, F. B. GUIMARAES, and L. C. LEAL

Oak Ridge National Laboratory, Oak Ridge, TN 37831-2008

Abstract

High-energy transport codes for the design of accelerator-driven systems such as the Spallation Neutron Source (SNS) use nuclear reaction models as the incident particle and the secondary particles are transported through various materials. These reaction models are computationally fast but are unreliable at energies below ~200 MeV. As a partial remedy, an evaluated cross-section library up to 150 MeV known as LA150 was developed by international cooperation and made available for such design work. In the present project we have been developing a model code suitable for improving LA150 and extending it to higher energies. This new model code combines microscopically the semiclasical results of an intranuclear-cascade model with the spin-dependent counterparts of a preequilibrium Hauser-Feshbach model. To achieve this microscopic combination, an approximation, explained in this paper, is needed to add spin distributions to the semiclassical excitation spectra in every residual nuclide. The initial capability of this code is demonstrated by comparisons with experimental production cross sections of the radioisotopes ^{56}Co, ^{55}Co, ^{54}Mn, ^{52}Mn, ^{52}Fe, ^{51}Cr, ^{48}Cr, ^{48}V, ^{47}Sc, and ^{46}Sc induced by proton projectiles on Fe from reaction thresholds to 3 GeV. The overall agreement of our calculated results with experimental data looks very good in view of the 29 contributions in a recent model code intercomparisons with measurements.

I. INTRODUCTION

High-energy transport codes such as MCNPX (Ref. 1) and HETC (Ref. 2) use nuclear reaction models to calculate needed cross sections as the incident and the secondary particles are transported through the target materials. For particle energies between 1 MeV and 5 GeV, the nuclear cross sections in these transport codes are calculated using the intranuclear cascade (INC), preequilibrium (PE), and evaporation models. These semiclassical models are computationally fast but are unreliable at incident energies below ~200 MeV where spin-dependent models are needed. As a partial remedy, an evaluated cross-section library called LA150 (Ref. 3), based on calculations using spin-dependent models, has been used in MCNPX to cover incident proton and neutron energies below 150 MeV for 15 materials. LA150 has been very useful; however, if the upper energy of 150 MeV could be extended to higher energies and the number of materials increased, then high-energy transport codes would provide better theoretical predictions of neutron production, shielding requirements, radioactive waste production, and radiation damage to materials. The objective of the work reported in this paper is to develop a nuclear model code that would be capable of improving LA150, extending it to higher energies, and including more materials. However, for incident energies between 150 MeV and 5 GeV, a large part of the decay processes still involves excitation energies below 150 MeV. Therefore, the semiclassical models still work poorly and are also incapable of generating production cross sections for isomeric states of fixed spin values, γ-ray transitions among discrete nuclear levels, spin-dependent γ-ray competition with nucleon emissions, and γ-ray production cross sections. We added these capabilities and achieved our objective by connecting microscopically the semiclassical results of an existing code to a spin-dependent code. Our new model code CETNG (for Cascade Exciton TNG) is capable of calculating pion production cross sections at the high-energy end of a decay chain as well as isomeric-state production cross sections and γ-ray production cross sections at the low-energy end of the same decay chain for an incident energy as high as 5 GeV, a feat no existing model code is capable of. Some initial results of the present project were documented as an ORNL report[4] and submitted for publication as a conference paper.[5] In the present paper we present refinements of CETNG, extend the maximum number of emitted particles from 6 to 12, include individual calculated components of the radioisotope production cross sections in the figures to understand structures in the measured data, and plot all available experimental data to see model problems objectively.

II. TECHNICAL APPROACH

Existing model codes and new approaches were used in the present effort to develop CETNG. The INC model and its related semiclassical PE model were taken from the CEM code, an ORNL version of CEM95 (Ref. 6). The Hauser-Feshbach (H-F) model and its related spin-dependent PE model were based on the TNG code (Ref. 7). The evaporation model and the low-energy end of the PE model of CEM were superceded by TNG, allowing measured discrete levels and their γ-ray branching ratios of every residual nuclide to play a role. To connect the semiclassical results of CEM with the spin-dependent results of TNG, we added spin distributions to the low-energy part of the CEM excitation spectra (cross sections as a function of excited states in each residual nuclide). The theories and

approximations used to accomplish this are described in detail in Refs. 4 and 5; however, our approach and refinements can be summarized as follows: For incident energies below 40 MeV, our code uses pure TNG. Between 40 MeV and 80 MeV, the TNG excitation spectra and the corresponding part of CEM are combined with a weight that favors TNG at 40 MeV and CEM at 80 MeV. The weight for TNG is 40/E and for CEM is 1-(40/E) where E is the incident energy in MeV. The combined excitation spectra are further de-excited quantum mechanically in TNG using the spin distributions calculated by TNG. For incident energies between 80 MeV and 5 GeV, the TNG excitation spectra obtained at 80 MeV are weighted downward by an additional 80/E before combining with the CEM excitation spectra obtained at any incident energy between 80 MeV and 5 GeV. This part of CETNG between 80 MeV and 5 GeV is further explained in the following paragraph.

Since the maximum incident energy of TNG is set to 80 MEV, how do we handle an incident energy of 5 GeV? Assume that after emitting the first particle in TNG for an incident energy of 80 MeV, the maximum excitation energy in the residual nuclide is also 80 MeV. After emitting a second particle, the maximum excitation energy in the new residual nuclide decreases by the reaction threshold (say 8 MeV) to 72 MeV. We extend it upward to 80 MeV and fill spin distributions of the extended energy range (8-MeV wide) by the spin distributions available at 72 MeV. We continue this extension for all additional particle emissions. This continuous extension makes spin distributions available in CETNG for new input CEM excitation spectra, the part of CEM below exciation energies of 80 MeV in any residual nuclide, to decay further in CETNG even if the incident energy is as high as 5 GeV. In other words, for any residual nuclide, the spin distributions below an excitation energy of 72 MeV are based on new calculations starting with an optical model suitable for the specific nuclide and the outgoing particle. Only the spin distributions between excitation energies of 72 and 80 MeV are based on the extension. This extension of spin distributions is the major approximation of CETNG.

A serious problem in CEM, emphasized by Gudima, Mashnik, and Toneev[8] and by Mashnik, Sierk, Bersillon, and Gabriel,[9] is the very low production cross sections of α-particles in all test cases. This problem results in discontinuities of a factor of 3 between some TNG and CEM cross sections involving α-particle emissions around 80 MeV in the present test case. To reduce these discontinuities, we increased the α-particle condensation probability, defined in Eq. 27 in Ref 8 and Eq. 17 in Ref. 9 and used in the PE component of CEM, by a factor of 10. To avoid confusion we call from here on the CEM version with this increased α-particle probability CEMX. The Fe(p,x)^{4}He cross sections using CEM and CEMX are compared in Fig. 1. The corresponding experimental data are from Michel et al.,[10] Schaeffer et al.,[11] Jung[12] and Green et al.[13] The CEMX α-particle production cross sections, though sharply increased over those of CEM, remain smaller than that from TNG at 80 MeV and also smaller than all the experimental data above 300 MeV. The CETNG cross sections, from combining TNG and CEMX, is larger than that of CEMX around 80 MeV because the TNG result at 80 MeV is larger. The CETNG result is only slightly greater than CEMX above 300 MeV. One could infer a factor-of-3 drop of the CETNG cross section above 80 MeV had the original CEM, rather than CEMX, been combined with TNG.

The increased α-particle production cross sections in CEMX reduced the competing t (or ^{3}H) and ^{3}He production cross sections, also shown in Fig. 1. These competing t, ^{3}He and ^{4}He production cross sections from CEMX appear to be a good compromise within the PE component in view of the experimental data shown. The experimental data are, for the ^{3}H productions, from Bogatin et. al.,[14] Mekhedov,[15] Fireman and Zahringer,[16] Currie,[17] Schaeffer and Zahringer[18] and Brun et al.,[19] and for the ^{3}He productions, from Michel et al.,[10] Schaeffer and Zahringer[11] and Green et al.[13] Further increases of the CEMX ^{4}He production cross sections shown in Fig. 1 are needed but can only be obtained by including them in the INC component assuming preformation of this particle, a difficult task that is beyond the scope of the present work. The PE components of the p, n, and d production cross sections in CEMX are also reduced, but to a smaller proportion because these three cross sections are larger. The total reductions on p and n productions are small in percentage because they also have large contributions from the INC components. We have not found any high-energy experimental deuterium production data to compare with, hence we are not sure whether the present CEMX modification is appropriate for deuterium production cross sections.

All experimental data shown in Fig. 1 and in the remaining figures were retrieved from the National Nuclear Data Center of Brookhaven National Laboratory and are labeled in each figure by the last name of the first author followed by the year the measurement was reported. Full names of all coauthors are cited in the references.

The calculated radioisotope production cross sections referred to as CETNG from here on were based on the combination of TNG and CEMX. Earlier results[4,5] from CETNG were based on the combination of TNG and CEM. The CETNG and CEMX outputs are deliberately made to be disjoint, so they can be summed for final results, including double differential spectra of all outgoing particles, γ-rays and pions. We were able to obtain, using CETNG, similar n and p double differential spectra calculated and used for the evaluated Fe data file in the LA150 library shown in Ref. 3. Such results, expected from those already obtained from TNG (Ref. 7) and CEM95 (Refs. 6,8,9), do not represent new results and are therefore not shown in this paper.

IV. RESULTS AND ACCOMPLISHMENTS

We pay particular attention to proton-induced radionuclide production cross sections because these data are widely measured in the energy range of interest and are challenging for model developers to calculate. As opposed to neutron and proton production cross sections and spectra, which are often the sums of many decay chains, the production of a single nuclide often involves a specific decay chain sensitive to specific properties and parameters (optical-model and level-density model parameters) used to describe that nuclide and the outgoing particle. When two or more decay modes contribute to the production of the same nuclide, such as ^{56}Fe(p,nα)^{52}Mn and ^{56}Fe(p,2p3n)^{52}Mn, they have widely spaced thresholds; therefore, model problems in each decay mode can be seen and studied separately. The reaction ^{56}Fe(p,nα)^{52}Mn has an outgoing α-particle, hence is sensitive to parameters used for α-particles.

The results shown below are preliminary because we are still in the developing phase

of CETNG and the model parameters we used were taken from defaults built into CEM and TNG without any careful determinations. Though preliminary, the results seem very encouraging. We mention only a few important parameters. The proton and neutron optical model parameters for TNG are from Table II of Chadwick et al.[3] and the α-particle parameters are from McFadden and Satchler.[20] The level-density parameters for CEM are from the third set (IFAM=9 and ISHA=2 in Mashnik[6]) of several sets given by Iljinov et al.[21] and for TNG from Mengoni and Nakajima,[22] both sets of parameters used the formalism of Ignatyuk et al.[23] The TNG code uses a library[24] of discrete levels, their spins and parities and γ-ray branching ratios. The TNG code processes this library using the Gilbert-Cameron method[25] to connect smoothly the level densities defined by the discrete levels with the level densities given by the Mengoni and Nakagima parameters. The discrete-level library was retrieved from the National Nuclear Data Center of Brookhaven National Laboratory. The TNG code also uses an automated Q-value subroutine taken from CEM95 in order to have identical Q-values for TNG and CEMX when their excitation spectra in every residual nuclide, created with a specific Q-value, are combined.

Using CETNG, our calculated production cross sections of the radioisotopes ^{56}Co, ^{55}Co, ^{54}Mn, ^{52}Mn,^{52}Fe, ^{51}Cr, ^{48}Cr, ^{48}V, ^{47}Sc and ^{46}Sc from Fe(p,x) reactions are compared with those measured with proton energies up to 3 GeV. The CEM excitation spectra below an excitation energy of $\sim$80 MeV for incident energies up to 150 MeV were normalized to total reaction cross sections evaluated in the LA150 library before sending to CETNG. The total reaction cross sections from CEM in this energy range are too low by up to 14%. For incident energies above 150 MeV, the total reaction cross sections calculated by CEM were not changed. The TNG code is used for incident proton energies below 40 MeV, while CETNG is used above 40 MeV. Calculated results using the targets of ^{56}Fe and ^{54}Fe were separately obtained and were summed with 92% and 5.8%, respectively, to represent natural Fe. Where ^{54}Fe contributions are important, they are shown individually in the figures. The two minor isotopes ^{57}Fe and ^{58}Fe have been ignored for the present phase of work. The comparisons of our calculated results with experimental data are further discussed in the following subsections.

The CEMX output of excitation spectra for each residual nuclide is designated with a reaction title, such as (p,ppn+dzpnag) where + is used to denote positively charged pion, d for deuteron, z for neutral pion, a for α and g for γ-ray, before sending to the matching part of CETNG for further decay. Since TNG and CETNG do not calculate d, t, ^{3}He and pion emissions, reactions with titles having these particles have to be dealt with to obtain their contributions to the radioisotope production cross sections and to conserve the total reaction cross section. Contributions to radioisotope productions from reactions with titles having d, t and ^{3}He are either extracted directly from the CEMX output when they are large or converted to protons and neutrons when they are small. Charged pions are combined with nucleons to conserve mass and charge of the relevant residual nuclide (for example, +n becomes p). Neutral pions are simply dropped from the reaction titles. Charge exchange reactions appear in the GeV range, but occur rarely, so they are ignored. Pion, d, t and ^{3}He production cross sections and spectra are obtained directly from the CEMX output where energy and direction of each outgoing particle are written. The present CETNG version only treats n, p, α and γ-ray explicitly while the sums d, t and

^{3}He cross sections are input as correction factors to conserve total reaction cross sections.

IV.A. ^{56}Fe(p,n)^{56}Co

We have assumed in the calculation that the production of ^{56}Co is completely from the ^{56}Fe(p,n) reaction. The calculated and experimental cross sections are shown in Fig. 2 in two groups in order to view overlaping experimental data. The top group was scaled upward by a factor of 10. Some of the measured data have been thinned to avoid blackened areas in the figure (as occurred in Fig. 1 of Ref. 5). Experimental error bars smaller than the plotted symbols are omitted. The experimental data shown are from Michel et al.,[26] Aleksandrov et al.,[27] Brodzinski et al.,[28] Rayudu, [29,30] Sudar and Qaim,[31] Schiekel et al.,[32] Lagunas-Solar and Jungerman,[33] Lavrukhina et al.,[34] Orth et al.[35] and Schoen et al.[36]

IV.B. ^{56}Fe(p,2n)^{55}Co

We have assumed in the calculation that the production of ^{55}Co is completely from the ^{56}Fe(p,2n) reaction, shown in Fig. 3. The measured data are from Michel et al.,[37] Lagunas-Solar and Jungerman,[33] Aleksandrov et al.,[27] Rayudu,[30] Lavrukhina et al.[34] and Orth et al.[35]

IV.C. ^{56}Fe(p,2pn)^{54}Mn

We have assumed in the calculation that the production of ^{54}Mn is completely from the ^{56}Fe(p,2pn) reaction, shown in Fig. 4. The data shown are from Brodzinski et al.,[28] Rayudu,[29,30] Schiekel et al.,[32] Schoen et al.,[36] Aleksandrov et al.,[27] Michel et al.,[37] Lavrukhina et al.,[34] Orth et al.[35] and Honda and Lal.[38] The calculated cross sections just above the threshold seem too low, we have not yet been able to understand why.

IV.D. Fe(p,x)^{52}Mn

The calculated data shown in Fig. 5 have a low-energy peak due to the ^{56}Fe(p,nα) reaction and a high-energy peak from ^{56}Fe(p,2p3n). The two reactions have widely spaced thresholds (2 outgoing particles versus 5), hence clearly separated peaks. The small contribution from ^{54}Fe(p,2pn) is important in the deep valley between the two peaks, but our calculated result appears too large. That these two sharp peaks are not seen in in Fig. 25 of Ref. 3 for the LA150 library seems strange but acceptable as an evaluation. However, understanding the origin of each peak and its rise and fall is important for the present model development. The experimental data are from Brodzinski et al.,[28] Rayudu,[29,30] Schiekel et al.,[32] Schoen et al.,[36] Lagunas-Solar and Jungerman,[33] Michel et al.,[26] Aleksandrov et al.,[27] Lavrukhina et al.,[34] Orth et al.[35] and Honda and Lal.[39]

IV.E. Fe(p,x)^{52}Fe

This is shown in Fig. 6. The calculated cross sections are sums of three components: ^{54}Fe(p,t+nd), ^{54}Fe(p,p2n), and ^{56}Fe(p,p4n). The ^{54}Fe(p,t+nd) component was extracted from CEMX and is important near the threshold. All three calculated components appear too small, especially the ^{56}Fe(p,p4n) component at high energies. We guess this is due to optical model parameters used presently in CETNG that underpredict each neutron emission slightly. When our calculated radionuclide production cross sections involve more neutrons than protons, such as in ^{56}Fe(p,p4n) here, the calculated cross sections tend to

be too small. The small underprediction of each neutron emission could build up after several consecutive neutron emissions. This might also be true for the underprediction of ^{48}Cr production cross sections discussed in subsection IV.G and the overprediction of ^{54}Fe(p,2pn)^{52}Mn discussed earlier in subsection IV.D. We would like to check this guess in the future. The measured data shown are from Michel et al.,[37,40] Aleksandrov et al.[27] and Orth et al.[35]

IV.F. Fe(p,x)^{51}Cr

This is shown in Fig. 7 and has three peaks. The 45-MeV peak is from the ^{56}Fe(p,pnα) reaction and the 90-MeV peak is from ^{56}Fe(p,3p3n). The measured data show a small peak below 30 MeV which is from the ^{54}Fe(p,p^{3}He) reaction. Our calculated results below 30 MeV were obtained directly from CEMX and are one decade smaller than the measured data and three decades smaller than the other two peaks, hence neglected in the figure. Included in the calculated ^{51}Cr production cross sections are small contributions from positron decays of ^{51}Mn via the ^{56}Fe(p,2nα+2p4n) reactions also shown in Fig. 7. The ^{51}Mn production cross sections also have two peaks, because they are the sums of two reactions with widely spaced thresholds. The experimental data are from Brodzinski et al.,[28] Rayudu,[29,30] Schiekel et al.,[32] Schoen et al.,[36] Honda and Lal,[38] Michel et al.,[26,37] Aleksandrov et al.,[27] Lavrukhina et al.[34] and Orth et al.[35]

IV.G. Fe(p,x)^{48}Cr

The CETNG results shown in Fig. 8 have three components: ^{54}Fe(p,p2nα), ^{56}Fe(p,p4nα) and ^{56}Fe(p,3p6n). Probably for the same reason given above for the calculated production cross sections of ^{52}Fe, the present calculated cross sections are smaller than most of the experimental data shown, especially the newest ones. The three steps seen in the calculated ^{48}Cr production cross sections, not obvious from the available experimental data, are likely to be real structures. The data shown are from Michel et al.,[10,41] Aleksandrov et al.,[27] Brodzinski et al.,[28] Rayudu,[30] Schiekel et al.,[32] Lavrukhina et al.[34] and Orth et al.[35]

IV.H. Fe(p,x)^{48}V

This is shown in Fig. 9. The two calculated components ^{56}Fe(p,n2α) and ^{54}Fe(p,2pnα) jointly contribute to the 55-MeV peak seen in the experimental data. Both calculated components involve the emission of an α-particle and are strongly influenced by TNG and by the increased α-particle production in CEMX shown in Fig. 1. The same peak seen in Fig. 36 of Mashnik et al.[8] using CEM95 is smaller by a factor of 10. The experimental data shown are from Brodzinski et al.,[28] Rayudu, [29,30] Schiekel et al.,[32] Schoen et al.,[36] Barchuk et al.,[42] Michel et al.,[37,10] Aleksandrov et al.,[27] Lavrukhina et al.[34] and Orth et al.[35]

IV.I. Fe(p,x)^{47}Sc

This is shown in Fig. 10. Our calculated 70-MeV peak is due to the ^{56}Fe(p,2p2α) reaction that is smaller than the data shown probably because this peak is quite small. Our past experience suggests that small cross sections are more difficult to predict because they are sensitive to errors in model parameters for large competing cross sections. Even

so, the present results remain an improvement over that calculated by Mashnik et al. using CEM95 (Fig. 37, Ref. 8) where the 70-MeV peak is not seen at all. The data shown are from Michel et al.,[10,43,40] Aleksandrov et al.,[27] Rayudu,[30] Schiekel et al.,[32] Lavrukhina et al.[34] and Orth et al.[35]

IV.J. Fe(p,x)^{46}Sc

This is shown in Fig. 11. Our calculation below 150 MeV represents a large improvement over that using CEM95 by Mashnik et al.(Fig. 37, Ref. 8) where the component ^{56}Fe(p,2pn2α) is not seen at all. The data shown are from Michel et al.,[10,43,40] Aleksandrov et al.,[27] Brodzinski et al.,[28] Schiekel et al.,[32] Lavrukhina et al.,[34] Orth et al.[35] and Honda and Lal.[38]

IV.K. CETNG versus CEM

Cross sections calculated with CETNG and with CEM for Fe(p,x)^{48}V, ^{46}Sc and ^{47}Sc are compared in Fig. 12. The CETNG cross sections are much larger than those of CEM below 200 MeV because both TNG and CEMX have larger α-particle emission probabilities than CEM has. And in the energy range below 200 MeV, cross sections having an α-particle component are the most important for the total Fe(p,x)^{48}V, ^{46}Sc and ^{47}Sc cross sections. The CETNG results shown in Fig. 12 are reproduced from those shown in Figs. 9, 10 and 11, where the theoretical components involving α-particle emissions are shown to exhibit the effects of these components. The CEM results shown in Fig. 12 are nearly identical to those shown in Mashnik et al.[9] using CEM95, and therefore, the present comparisons between CETNG and CEM also represent comparisons between CETNG and CEM95.

IV.L. CETNG versus LA150

Fig. 13 shows comparisons of the Fe(p,x)^{48}V, ^{46}Sc and ^{47}Sc cross sections calculated with CETNG and with those calculated by Chadwick et al.[3] using the GNASH code (Ref. 44) and adopted for the LA150 data library. The three LA150 cross sections shown are mostly much larger than those of CETNG. As seen from Fig. 12 that compares the same cross sections from CETNG with those using CEM, the CEM results are much smaller below 150 MeV. Therefore, the differences between these LA150 data and the CEM results below 150 MeV are very large indeed. Because CEM is probably the best cross-section module within MCNPX, using LA150 in MCNPX does not solve all the cross-section problems in MCNPX, and LA150, as useful as it already is, still needs to be improved below 150 MeV and extended to higher energies.

As seen in the foregoing figures, some disagreements between our CETNG results with measured data exist. However, even with these disagreements, our results are still very good in view of the larger disagreements and limited energy ranges seen in the 29 contributions to a model code intercomparison with experimental data compiled by Michel and Nagel.[45] Well-known codes such as GNASH (Ref. 44), ALICE (Ref. 46) and CEM95 were represented. Large improvements over CEM95 for the production cross sections of ^{4}He are shown in Fig. 1. Improvements over CEM (and CEM95) and LA150 for the production cross sections of ^{48}V, ^{47}Sc and ^{46}Sc are shown in Figs. 12 and 13, respectively. As seen in one of our earliest demonstration[47] of TNG, we are proficient in calculating

γ-ray production cross sections, especially the parts sensitive to discrete-level spin values (see Fig. 26 of Ref. 47). In addition, TNG has been used with success for many evaluated double differential cross sections in the ENDF/B-VI neutron data files.[48] Likewise CEM95 (CEM and more so CEMX) is a powerful high-enegy code validated extensively.[9,49] Our new code CETNG makes good use of these TNG and CEM95 capabilities for incident energies as high as 5 GeV by starting a decay chain using the INC model of CEMX and ending it with the H-F model in TNG.

V. DISCUSSIONS

Our work described in the foregoing sections originated from the observation that a radioisotope is formed when the excited states in this isotope become particle-stable. The energy range of such particle-stable states is between the ground state and ~8 MeV, an energy range for which the discrete levels, their spins and parities and γ-ray branching ratios are known to play an important role in calculating the competitions between γ-ray and particle emissions. Such discrete-level information has been commonly used in H-F model codes such as GNASH and TNG, providing cross sections for exciting all discrete levels and γ-ray production cross sections showing sharp peaks due to γ-ray transitions between discrete levels.[47] By combining TNG and CEM, we obtain all such information from TNG in addition to other important results, such as direct knockout reactions, multiple particle emissions and pion productions, from the INC model in CEM. We believe we have successfully demontrated the feasibility of this idea, though more work remains.

One difficulty we have encountered is the long computer time needed to run CETNG. It uses an in-house optical model called for every combination of the mass and charge of a residual nuclide and the mass, charge, spin and energy of an outgoing particle. After each time an optical model is called, CETNG performs additional calculations to obtain various quantities that couple the optical-model transmission coefficients with the spin-dependent level densities and discrete levels with conservation of all spin values. This is where the computer time goes. This approach is fine at low incident energies but at high incident energies the same combination ocurred hundreds of times. Therefore, we need to store all such quantities the first time a combination is encountered and then use them repeatedly. We have started implementing this procedure. Improved computer efficiency will allow us to calculate a larger number (currently 12) of emitted particles without being handicapped by long computer hours.

Lillie and Gallmeier[50] have developed a coupled neutron and photon library, HILO2k, for neutron energies up to 2 GeV. This library is intended for use in discrete-ordinate transport codes. Of particular interest to the present work is that there exist discontinuities across 150 MeV in many cross sections between this library and LA150. Because HILO2k was primarily derived from the cross-section modules within MCNPX, these discontinuities also represent discontinuities at 150 MeV between MCNPX and LA150. This means there is an urgent need to extend LA150 to higher energies. The present CETNG code is capable of meeting such a need.

Koning, Delaroche, and Bersillon[51] have evaluated 150-MeV neutron and proton transport data files for ^{54}Fe, ^{56}Fe, ^{58}Ni and ^{60}Ni. Their optical-model parameters simulate the

dispersive effects at low energy and can be used consistently from 1 MeV to 200 MeV. We intend to adopt this set of parameters for our next phase of CETNG development.

As mentioned earlier that CEM is an ORNL version of CEM95. We made some minor changes to CEM95 by making it run with fewer infinite cycles, including the use of a new random number generator. We added subroutines to extract cross sections for reactions such as (p,t) and (p,dn) shown in Fig. 6. CEM has been used to combine with TNG in our earlier publications[4,5] while CEMX, having a sharply increased α-particle production, is used for the calculated results presented here. For this reason, the calculated results presented here are somewhat different from those given earlier. The code names CEM95, CEM and CEMX are used only in this paper to avoid confusion. The authors of CEM95[6,8,9] have been improving this code and calling the improved versions with various suffixes.

VI. WORK IN PROGRESS

As mentioned in Sec. IV, CEM uses one of the level density models given by Iljinov et al.[21] while TNG has a similar level-density model from Mengoni and Nakajima[22]; however, TNG modifies the low energy part by taking into account the available discrete levels using the Gilbert and Cameron formalism.[25] The TNG approach is more reliable at low excitation energies because the known discrete levels better define odd-even effects than do level density models. We have started unifying the level-density models in the two codes by using the number of discrete levels (of all nuclides available in the discrete level library) up to a certain excitation energy as a constraint to level-density parameter values in CEMX and by making both models available in CEMX, TNG and CETNG. The new CEMX with the improved level density formalism, together with the improved α-particle emission, will be installed in HETC to replace CEM95 currently available there.

As also mentioned earlier we have started improving the computer efficiency by storing some tediously calculated parts the first time a combination of a residual nuclide and an outgoing particle is encountered and then using them repeatly. After completing this, we will be able to add d, t, ^{3}He emissions to TNG and CETNG and to calculate all the decay chains to the end. These developments demand efficient programming.

VII. SUMMARY AND CONCLUSIONS

Our new model code CETNG described in this paper is based on a microscopic combination of INC, PE, and H-F models. CETNG starts a decay chain with the INC model, passes through the PE model, and ends with the H-F model. It is therefore capable of producing multiple particle emissions and pion productions at the high-energy end of a decay chain, and cross sections for exciting discrete levels (and therefore for isomeric states) of fixed spin values and for gamma-ray transitions among discrete levels at the low-energy end of the same decay chain. In this paper we compared our calculated production cross sections for 10 radioisotopes from proton projectiles on Fe with all available measured data, instead of just Michel et al.[26] as in our earlier report,[5] to judge our model problems more objectively. We plotted individual theoretical components for the production cross sections of each radioisotope to interpret measured data and to help understand model problems for each individual component. We improved α-particle production cross sections in CEM

using TNG results of incident energies between 40 and 80 MeV as a guide. With this improvement, we achieved much better agreement with experimental data for the production cross sections of ^{46}Sc, ^{47}Sc, and ^{48}V for incident proton energies from thresholds to 200 MeV. In this energy range these three production cross sections are sensitive to α-particle emissions.

In Mashnik et al.[49], a narrative summary of Ref. 9 having hundreds of figures, a list of high-priority improvements for CEM95 includes "modeling the emission of gammas competing with the evaporation of particles at the compound stage" and "treating more accurately α-emission at the pre-equilibrium stage". These two recommended improvements have been reasonably met in the development of CETNG. Though we are continuing the development of CETNG, it can already be used together with CEMX for cross-section evaluation purposes. We intend to apply CETNG to extend the LA150 library to higher energies and to add more materials. This is ambitious and requires international cooperation (possibly with authors of Refs. 3, 8, 9, and 51) for years. As mentioned in Sec. VI, we have started improving the level density model used in CEMX by making use of the discrete level library already used in TNG, then installing the new CEMX in HETC to replace the CEM95 already in there.

ACKNOWLEDGMENTS

Research sponsored in part by the Laboratory Directed Research and Development Program of Oak Ridge National Laboratory (ORNL), managed by UT-Battelle, LLC for the U.S. Department of Energy (DOE) under Contract No. DE-AC05-00OR22725, and in part by other DOE funds. We appreciate helpful comments from our respected colleagues T. A. Gabriel, D. C. Larson, R. A. Lillie, R. W. Roussin, N. M. Larson, and B. L. Kirk.

REFERENCES

1 H. G. HUGHES, R. E. PRAEL, and R. C. LITTLE, "MCNPX - The LAHET/MCNP Code Merger," XTM-RN(U) 96-012, Los Alamos National Laboratory (1997).

2 H. W. BERTINI, *Phys. Rev.*, **188**, 1711 (1969); additional references and latest improvements of HETC in C. Y. FU and T. A. GABRIEL, "CALOR As A Single Code Including A Modular Version of HETC,", *Proc. 4th Workshop On Simulating Accelerator Radiation Environments (SARE4)*, Knoxville, TN, Sep. 14-16, p. 23, T. A. Gabriel, Ed., Oak Ridge National Laboratory (1998).

3 M. B. CHADWICK, P. G. YOUNG, S. CHIBA, S. C. FRANKLE, G. M. HALE, H. G. HUGHES, A. J. KONING, R. C. LITTLE, R. E. MacFARLANE, R. E. PRAEL, and L. S. WATERS, *Nucl. Sci. Eng.*, **131**, 293 (1999).

4 F. B. GUIMARAES, C. Y. FU, L. C. LEAL, "Combining Semi-Classical and Quantum Mechanical Methodologies for Nuclear Cross-Section Calculations between 1 MeV and 5 GeV ", ORNL/TM-2001/191 (ENDF-366), Oak Ridge National Laboratory (2001).

5 C. Y. FU, F. B. GUIMARAES, and L. C. LEAL, "Combining Semiclassical and Quantum Mechanical Methodologies For Nuclear Cross-Section Calculations between 1 MeV and 5 GeV," International Conference on Nuclear Data for Science and Technology, Tsukuba, Japan, Oct. 7-12, 2001. Full paper to be published in a special issue of the Journal of Nuclear Science and Technology (Japan).

6 S. G. MASHNIK, "User's Manual for the Code CEM95", unpublished report, Bogoliubov Laboratory of Theoretical Physics, Joint Institute of Nuclear Physics, Moscow Region, Russia, 1995, Personal Communication to T. A. GABRIEL and C. Y. FU, 1996.

7 C. Y. FU, *Nucl. Sci. Eng.*, **100**, 61 (1988); also K. SHIBATA and C. Y. FU, "Recent Improvements of the TNG Statistical Model Code," ORNL/TM-10093, Oak Ridge National Laboratory (1986).

8 K. K. GUDIMA, S. G. MASHNIK and V. D. TONEEV, *Nucl. Phys. A*, **401**, 329 (1983).

9 S. G. MASHNIK, A. J. SIERK, O. BERSILLON, T. A. GABRIEL, "Cascade-Exciton Model Detailed Analysis for Proton Spallation at Energies from 10 MeV to 5 GeV," LA-UR-97-2905, Los Alamos National Laboratory (1997).

10 R. MICHEL, M. GLORIS, H. LANGE, I. LEYA, M. LUEPKE, U. HERPERS, B. DITTRICH-HANNEN, R. ROSEL, Th. SCHIEKEL, D. FILGES, P. DRAGOVITSCH, M. SUTER, H.-J. HOFMANN, W. WOLFLI, P. KUBIK, H. BAUER, and R. WIELER, *Nucl. Inst. Meth. Phys. B*, **103**, 183 (1995).

11 O. A. SCHAEFFER and J. ZAHRINGER, *Phys. Rev.*, **113**, 674 (1959).

12 P. JUNG, *J. Nucl. Materials*, **144**, 43 (1987).

13 S. L. GREEN, W. V. GREEN, H. HEGEDUS, M. VICTORIA, W. F. SOMMER, and B. M. OLIVER, *J. Nucl. Materials*, **155/157**, 1350 (1988).

14 V. I. BOGATIN, V. F. LITVIN, O. V. LOZHKIN, N. A. PERFILOV, and YU. P. YAKOVLEV, *Nucl. Phys. A*, **260**, 446 (1976).

15 V. N. MEKHEDOV, *Yad. Fiz. (Russia)*, **5**, 34 (1967).

16 E. L. FIREMAN and J. ZAHRINGER, *Phys. Rev.*, **107**. 1695 (1957).

17 L. A. CURRIE, *Phys. Rev.*, **114**, 878 (1959).

18 O. A. SCHAEFFER and J. ZAHRINGER, *Z. Naturforsch. A*, **13**, 346 (1958).
19 P. C. BRUN, M. LEFORT, X. TARRAGO, *J. Physique (France)*, **248**, 3552 (1959).
20 L. McFADDEN and G. R. SATCHLER, *Nucl. Phys.*, **84**, 177 (1966).
21 A. S. ILJINOV, M. V. MEBEL, N. BIANCHI, E. De. SANCTIS, C. GUARDALO, V. LUCHERIINI, V. MUCCIFORA, E. POLLI, A. R. REOLON, and P. ROSSI, *Nucl. Phys. A*, **543**, 517 (1992).
22 A. MENGONI and Y. NAKAJIMA, *J. Nucl. Sci. Eng. (Japan)*, **31**(2), 151 (1994), and Personal Communication from A. MENGONI to C. Y. FU, 1995.
23 A. V. IGNATYUK, N. SMIRENKIN, and A. S. TISHIN, *Sov. J. Nucl. Phys.*, **21**, 255 (1975).
24 "Handbook for calculations of nuclear reaction data, Reference input parameter library", IAEA-TECDOC-1034, International Atomic Energy Agency, Vienna, Austria (1998), File *Beijing.dat*, Provided by Su Zondi, as of 1 February 1996, Chinese Nuclear Data Center, CIAE, Beijing, China, Retrieved from *http://www.nndc.bnl.gov*
25 A. GILBERT and A. G. W. CAMERON, *Can. J. Phys.*, **43**, 1446 (1965).
26 R. MICHEL, B. DITTRICH, U. HERPERS, F. PEIFFER, T. SCHIFFMANN, P. CLOTH, P. DRAGOVITSCH, D. FILGES, *Analyst (London)*, **114**, 287 (1989).
27 Yu. V. ALEKSANDROV, A. I. BOGDANOV, S. K. VASILJEV, R. B. IVANOV, M. A. MIKHAILOVA, T. I. POPOVA, and V. P. PRIKHODTZEVA, *Izv. Kaz. Akad. Nauk, Ser. Fiz. (Karzarkstan)*, **54**, 2249 (1990).
28 R. L. BRODZINSKI, L. A. RANCITELLI, J. A. COOPER, and N. A. WOGMAN, *Phys. Rev. C*, **4**, 1257 (1971).
29 G. V. S. RAYUDU, *Can. J. Chem.*, **42**, 1149 (1964).
30 G. V. S. RAYUDU, *Inorg. Nucl. Chem. Lett. (UK)*, **30**, 2311 (1968).
31 S. SUDAR and S. M. QAIM, *Phys. Rev. C*, **50**, 2408 (1994).
32 Th. SCHIEKEL, F. SUDBROCK,U. HERPERS, M. GLORIS, H.-J. LANGE, I. LEVA, R. MICHEL, B. DITTRICH-HANNEN, H.-A. SYNAL, M. SUTER, P. W. KUBIK, M. BLANN, and D. FILGES, *Nucl. Inst. Meth. Phys. B*, **114**, 91 (1996).
33 M. C. LAGUNAS-SOLAR and J. A. JUNGERMAN, *Radiochimica Acta (Germany)*, **60**, 57 (1979).
34 A. K. LAVRUKHINA, A. D. REVINA, V. V. MALYSHEV, and L. M. SATAROVA, *Zhur. Eksp. Teor. Fiz. (Russia)*, **44**, 1429 (1963).
35 C. H. ORTH, H. A. O'BRIEN Jr., M. E. SCHILLACI, B. J. DROPESKY, J. E. CLINE, E. B. NIESCHMIDT, and R. J. BROZINSKI, *Inorg. Nucl. Chem. Lett. (UK)*, **38**, 13 (1976).
36 N. C. SCHOEN, G. ORLOV, R. J. McDONALD, *Phys. Rev. C*, **20**, 88 (1979).
37 R. MICHEL, G. BRINKMANN, H. WEIGEL, and W. HERR, *Nucl. Phys. A*, **322**, 40 (1979).
38 M. HONDA and D. LAL, *Nucl. Phys.*, **51**, 363 (1964).
39 M. HONDA and D. LAL, *Phys. Rev.*, **118**, 1618 (1960).
40 R. MICHEL, M. GLORIS, H. LANGE, I. LEYA, M. LUEPKE, U. HERPERS, B. DITTRICH-HANNEN, R. ROSEL, Th. SCHIEKEL, D. FILGES, P. DRAGOVITSCH, M. SUTER, H.-J. HOFMANN, W. WOLFLI, P. KUBIK, H. BAUER, R. WIELER, *Nucl. Inst. Meth. Phys. B*, **129**, 153 (1997).

41 R. MICHEL, P. DRAGOVITSCH, P. ENGNERT, F. PEIFFER, R. STUEK, S. THEIS, F. BEGEMANN, H. WEBER, P. SIGNER, R. WIELER, D. FILGES, P. CLOTH, *Nucl. Inst. Meth. B*, **16**, 61 (1986).

42 I. V. BARCHUK, V. S. BULKIN, V. A. KUZMENKOVA, P. M. KURILO, Yu. N. LOBACH, A. F. OGORODNIK, V. S. PROCOPENKO, V. D. SKLYARENKO, V. V. TOKAREVSKY, *Atomnaya Energiya (Russia)*, **63**, 30 (1987).

43 R. MICHEL, F. PEIFFER, R. STUEK, *Nucl. Phys. A*, **441**, 617 (1985).

44 P. G. YOUNG, E. D. ARTHUR, and M. B. CHADWICK, "Comprehensive Nuclear Model Calculations: Theory and Use of the GNASH code", LA-12343-MS, Los Alamos National Laboratory (1992).

45 R. MICHEL and P. NAGEL, "International Codes and Model Intercomparisons for Intermediate Energy Activation Yields", NSC/DOC(97)-1, Nuclear Energy Agency, Organisation for Economic Co-operation and Development, Paris, France, 1997.

46 M. BLANN, "ALICE 92", UCRL-JC-109052, Lawrence Livermore National Laboratory (1991).

47 C. Y. FU, *Atom. Data Nucl. Data Tables*, **17**, 127 (1976).

48 "ENDF-201 ENDF/B-VI Summary Documentation", Compiled and Edited by P. F. Rose, BNL-NCS-17451, National Nuclear Data Center, Brookhaven National Laboratory (1991).

49 S. G. MASHNIK, A. J. SIERK, O. BERSILLON, T. A. GABRIEL, *Nucl. Inst. Meth. Phys. A*, **141**, 68 (1998).

50 R. A. LILLIE and F. X. GALLMEIER, "HILO Transport Cross-Section Library Extension", *Proc. 3rd Intl. Top. Mt. Nucl. Appl. Accl. Tech.*, Long Beach, CA, Nov. 14-18, 1999; also "HILO2k: A Coupled Neutron-Photon Transport Cross-Section Library for Neutron Energies up to 2000 MeV", *Proc. 4th Intl. Top. Mt. Nucl. Appl. Accl. Tech.*, Washinton DC, Nov. 12-16, 2000; and Personal Communication from R. A. LILLIE to C. Y. FU, 2001.

51 A. J. KONING, J. P. DELAROCHE, O. BERSILLON, *Nucl. Inst. Meth. Phys. A*, **414**, 49 (1998).

FIGURE CAPTIONS

Fig. 1. Cross sections Fe(p,x)t, He-3 and He-4 calculated using the CEM and CEMX codes are compared with experimental data. The CETNG result for He-4 production, from combining TNG and CEMX, is shown as the dashed curve that merges with CEMX above 300 MeV. The experimental data for He-4 productions are from Michel et al.,[10] Schaeffer et al.,[11] Jung[12] and Green et al.[13] and those for tritium productions are from Bogatin et. al.,[14] Mekhedov,[15] Fireman and Zahringer,[16] Currie,[17] Schaeffer and Zahringer[18] and Brun et al.[19] and those for He-3 productions are from Michel et al.,[10] Schaeffer and Zahringer[11] and Green et al.[13]

Fig. 2. Cross sections ^{56}Fe(p,n)^{56}Co are shown in two groups in order to view overlaping experimental data. The top group was scaled upward by a factor of 10. The experimental data are from Michel et al.,[26] Aleksandrov et al.,[27] Brodzinski et al.,[28] Rayudu,[29,30] Sudar and Qaim,[31] Schiekel et al.,[32] Lagunas-Solar and Jungerman,[33] Lavrukhina et al.,[34] Orth et al.[35] and Schoen et al.[36]

Fig. 3. Cross sections ^{56}Fe(p,2n)^{55}Co are shown in two groups in order to view overlaping experimental data. The top group was scaled upward by a factor of 10. The experimental data are from Michel et al.,[37] Lagunas-Solar and Jungerman,[33] Aleksandrov et al.,[27] Rayudu,[30] Lavrukhina et al.[34] and Orth et al.[35]

Fig. 4. Cross sections ^{56}Fe(p,2pn)^{54}Mn are shown in two groups in order to view overlaping experimental data. The top group was scaled upward by a factor of 10. The experimental data are from Brodzinski et al.,[28] Rayudu,[29,30] Schiekel et al.,[32] Schoen et al.,[36] Aleksandrov et al.,[27] Michel et al.,[37] Lavrukhina et al.,[34] Orth et al.[35] and Honda and Lal.[38]

Fig. 5. Cross sections Fe(p,x)^{52}Mn are shown in two groups in order to view overlaping experimental data. The top group was scaled upward by a factor of 10. The low-energy peak is due to the ^{56}Fe(p,nα) reaction and the high-energy peak is from ^{56}Fe(p,2p3n). The ^{54}Fe(p,2pn) cross section fills the valley between the two peaks. The experimental data shown are from Brodzinski et al.,[28] Rayudu,[29,30] Schiekel et al.,[32] Schoen et al.,[36] Lagunas-Solar and Jungerman,[33] Michel et al.,[26] Aleksandrov et al.,[27] Lavrukhina et al.,[34] Orth et al.[35] and Honda and Lal.[39]

Fig. 6. Cross sections Fe(p,x)^{52}Fe. The calculated cross sections are sums of three components: ^{54}Fe(p,t+nd), ^{54}Fe(p,p2n) and ^{56}Fe(p,p4n). The measured data shown are from Michel et al.,[37,40] Aleksandrov et al.[27] and Orth et al.[35]

Fig. 7. Cross sections Fe(p,x)^{51}Cr are shown in two groups in order to view overlaping experimental data. The top group was scaled upward by a factor of 10. The low-energy peak is due to the ^{56}Fe(p,pnα) reaction and the high-energy peak is from ^{56}Fe(p,3p3n). The small component is from positron decays of ^{51}Mn via the ^{56}Fe(p,2nα+2p4n) reactions. The experimental data are from Brodzinski et al.,[28] Rayudu,[29,30] Schiekel et al.,[32] Schoen et al.,[36] Honda and Lal,[38] Michel et al.,[26,37] Aleksandrov et al.,[27] Lavrukhina et al.[34] and Orth et al.[35]

Fig. 8. Cross sections Fe(p,x)^{48}Cr. The calculated results are sums of three components: ^{54}Fe(p,p2nα), ^{56}Fe(p,p4nα) and ^{56}Fe(p,3p6n). The data shown are from Michel et al.,[10,41] Aleksandrov et al.,[27] Brodzinski et al.,[28] Rayudu,[30] Schiekel et al.,[32] Lavrukhina et al.[34] and Orth et al.[35]

Fig. 9. Cross sections Fe(p,x)^{48}V. The two calculated components ^{56}Fe(p,n2α) and ^{54}Fe(p,2pnα) jointly contribute to the 55-MeV peak seen in the experimental data. The calculated component ^{56}Fe(p,2p3nα) contributes to the sharp rise seen in the experimental data at 100 MeV. The fourth component ^{56}Fe(p,4p5n) is important at high incident energies. The experimental data are from Brodzinski et al.,[28] Rayudu,[29,30] Schiekel et al.,[32] Schoen et al.,[36] Barchuk et al.,[42] Michel et al.,[37,10] Aleksandrov et al.,[27] Lavrukhina et al.[34] and Orth et al.[35]

Fig. 10. Cross sections Fe(p,x)^{47}Sc. The calculated results are sums of three components: ^{56}Fe(p,2p2α), ^{56}Fe(p,4p2nα) and ^{56}Fe(p,6p4n). The experimental data are from Michel et al.,[10,43,40] Aleksandrov et al.,[27] Rayudu,[30] Schiekel et al.,[32] Lavrukhina et al.[34] and Orth et al.[35]

Fig. 11. Cross sections Fe(p,x)^{46}Sc. The calculated results are sums of three components: ^{56}Fe(p,2pn2α), ^{56}Fe(p,4p3nα) and ^{56}Fe(p,6p5n). The experimental data are from Michel et al.,[10,43,40] Aleksandrov et al.,[27] Brodzinski et al.,[28] Schiekel et al.,[32] Lavrukhina et al.,[34] Orth et al.[35] and Honda and Lal.[38]

Fig. 12. Comparisons of the calculated Fe(p,x)^{48}V, ^{46}Sc and ^{47}Sc cross sections using CETNG with those using CEM. The cross sections calculated using CETNG are compared with experimental data in Figs. 9, 10 and 11, respectively. Those calculated with CEM are nearly identical to those calculated by Mashnik et al.[9] using CEM95.

Fig. 13. Comparisons of the Fe(p,x)^{48}V, ^{46}Sc and ^{47}Sc cross sections calculated using CETNG with those calculated by Chadwick et al.[3] using GNASH (Ref. 44) and adopted for the LA150 data library. The cross sections calculated using CETNG are compared with experimental data in Figs. 9, 10 and 11, respectively, and are compared with those using CEM in Fig. 12.

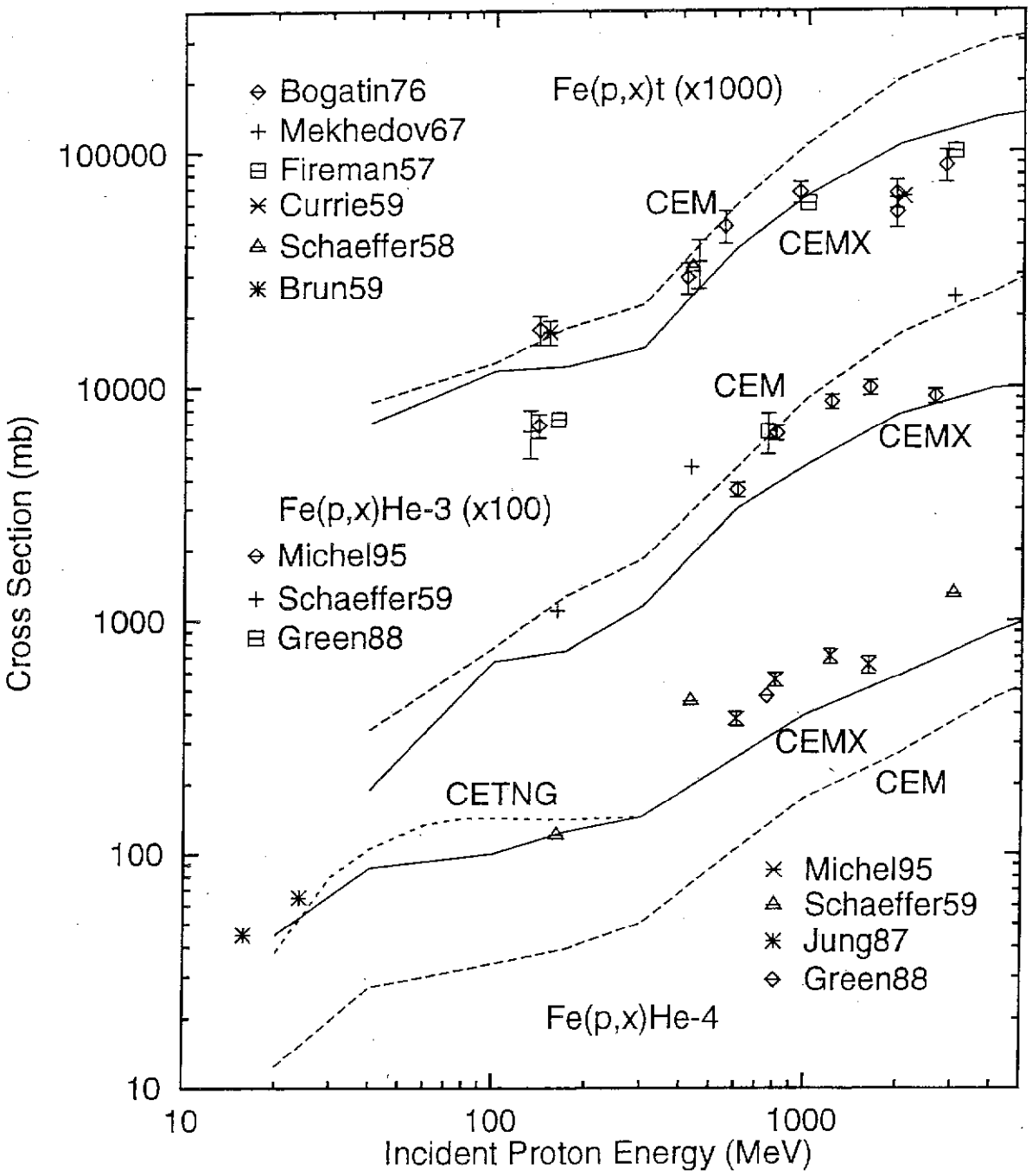

Fig. 1. Cross sections Fe(p,x)t, He-3 and He-4 calculated using the CEM and CEMX codes are compared with experimental data. The CETNG result for He-4 production, from combining TNG and CEMX, is shown as the dashed curve that merges with CEMX above 300 MeV. The experimental data for He-4 productions are from Michel et al.,[10] Schaeffer et al.,[11] Jung[12] and Green et al.[13] and those for tritium productions are from Bogatin et. al.,[14] Mekhedov,[15] Fireman and Zahringer,[16] Currie,[17] Schaeffer and Zahringer[18] and Brun et al.[19] and those for He-3 productions are from Michel et al.,[10] Schaeffer and Zahringer[11] and Green et al.[13]

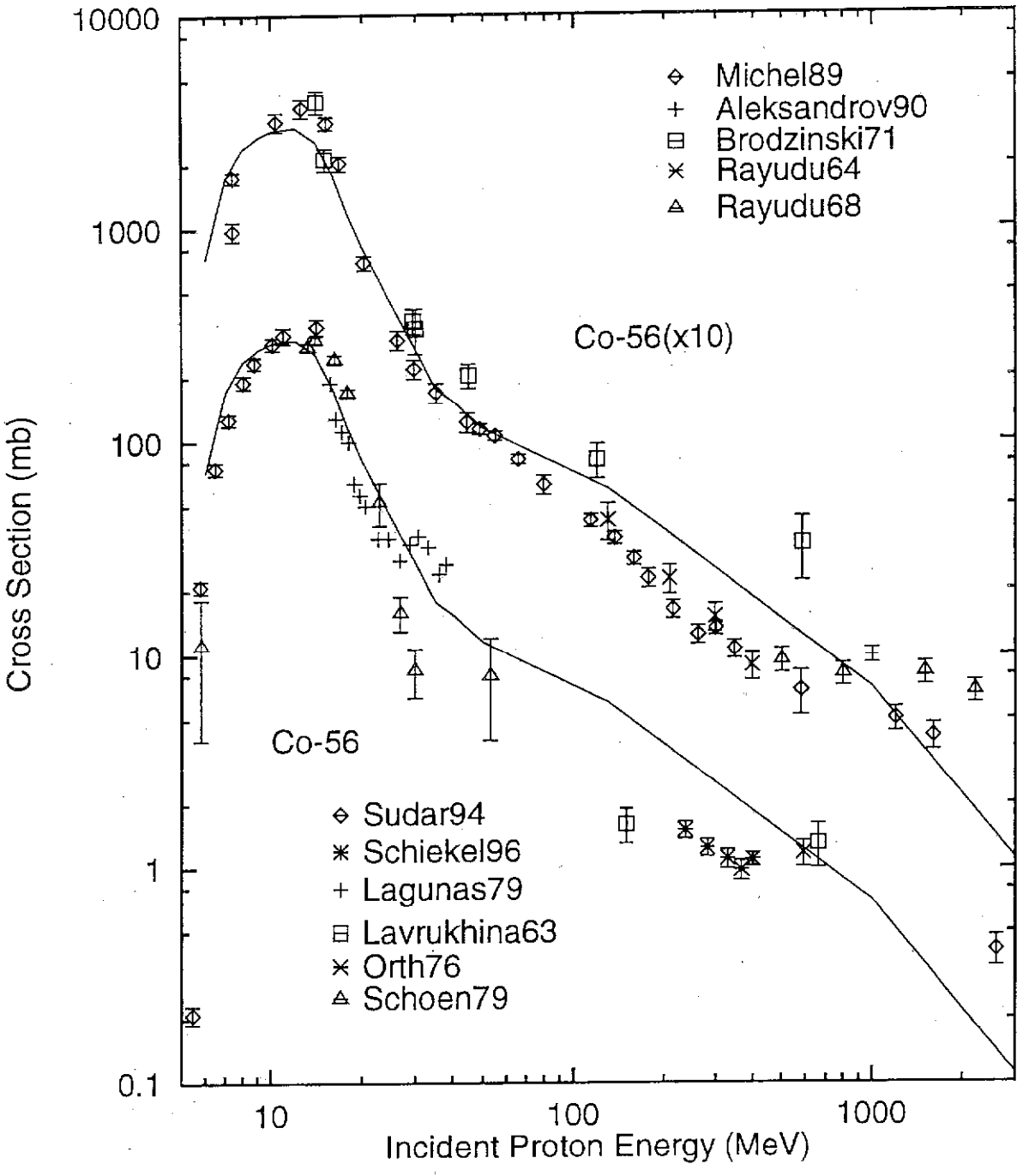

Fig. 2. Cross sections ^{56}Fe(p,n)^{56}Co are shown in two groups in order to view overlaping experimental data. The top group was scaled upward by a factor of 10. The experimental data are from Michel et al.,[26] Aleksandrov et al.,[27] Brodzinski et al.,[28] Rayudu,[29,30] Sudar and Qaim,[31] Schiekel et al.,[32] Lagunas-Solar and Jungerman,[33] Lavrukhina et al.,[34] Orth et al.[35] and Schoen et al.[36]

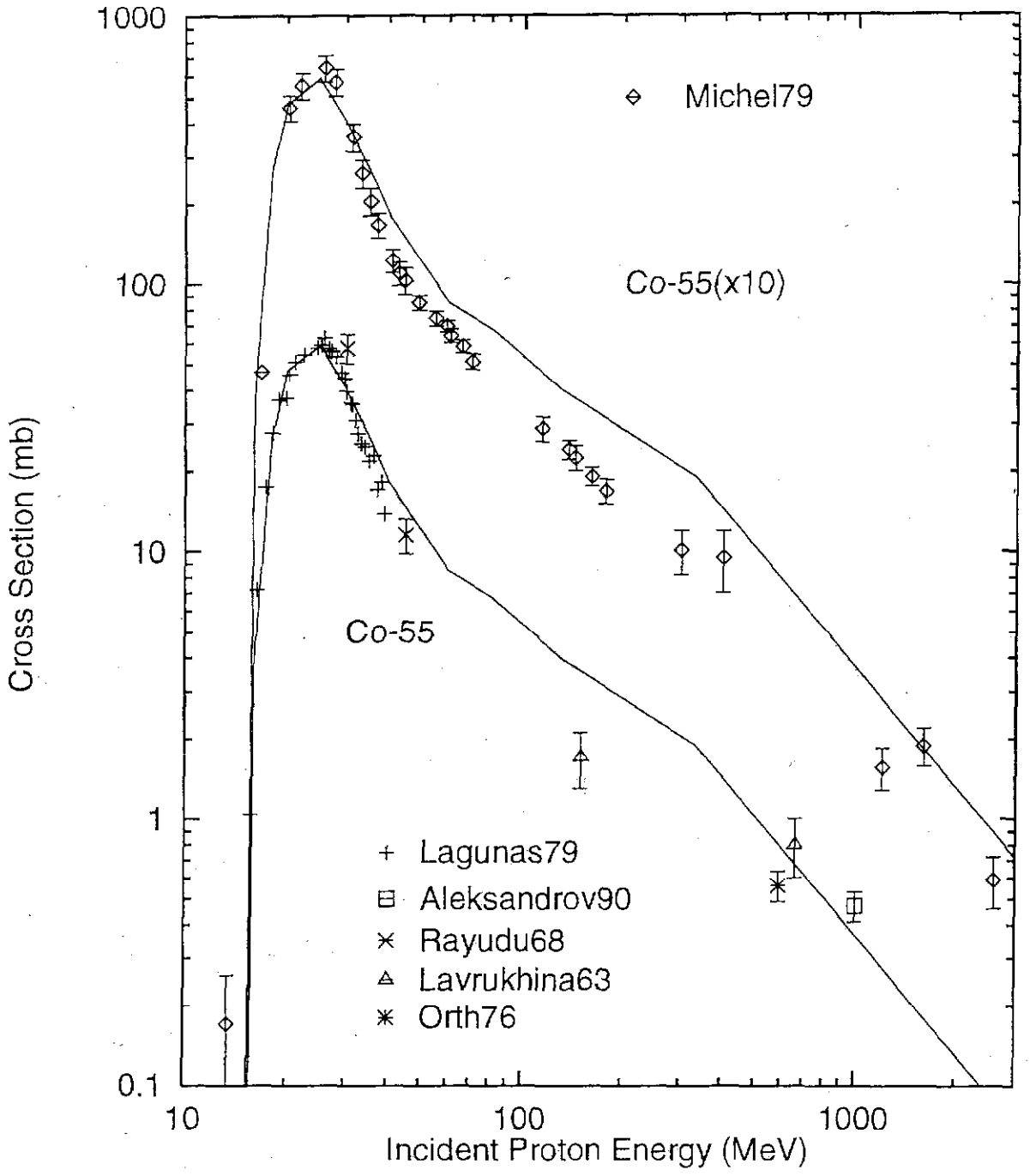

Fig. 3. Cross sections ^{56}Fe(p,2n)^{55}Co are shown in two groups in order to view overlaping experimental data. The top group was scaled upward by a factor of 10. The experimental data are from Michel et al.,[37] Lagunas-Solar and Jungerman,[33] Aleksandrov et al.,[27] Rayudu,[30] Lavrukhina et al.[34] and Orth et al.[35]

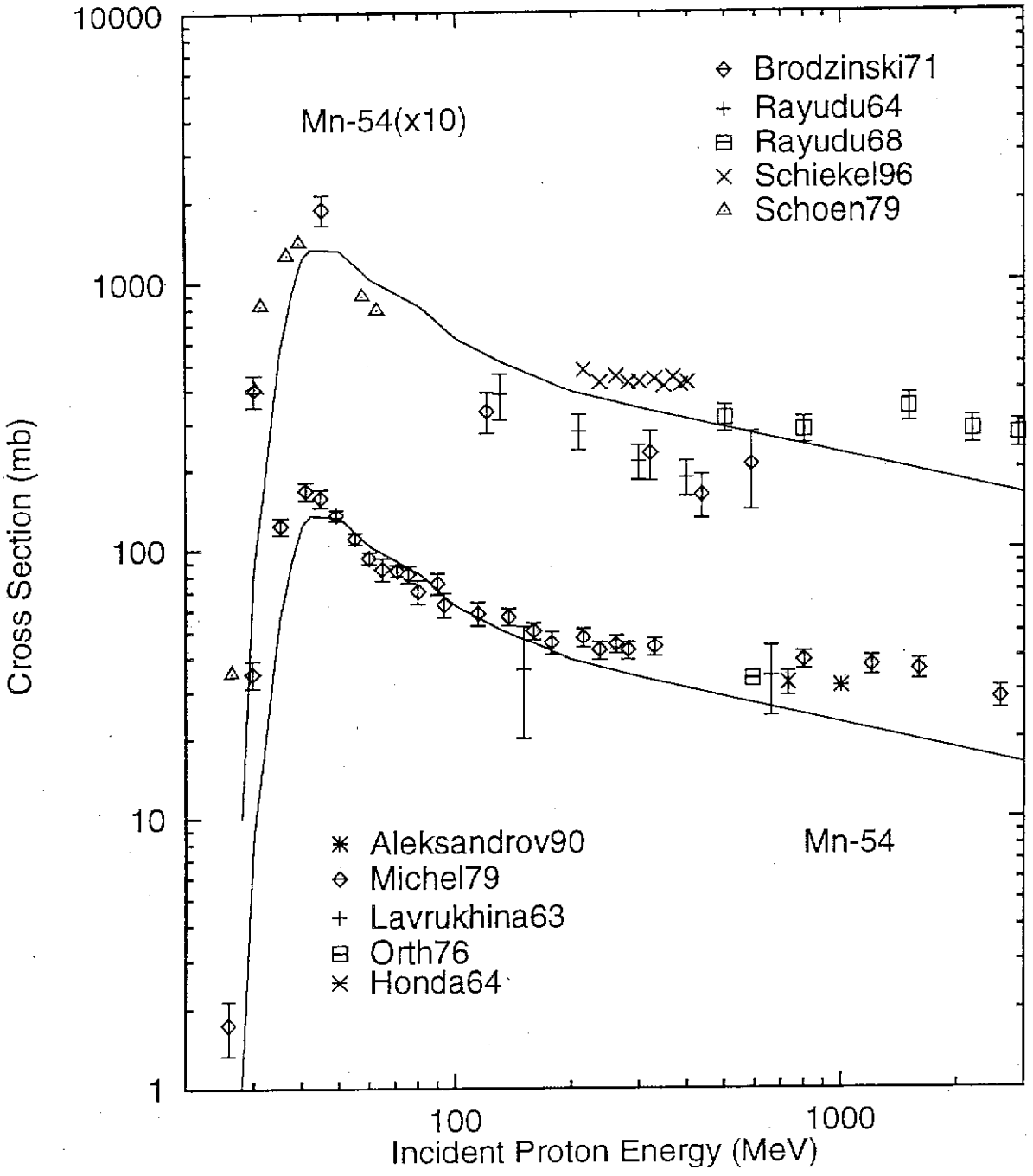

Fig. 4. Cross sections ^{56}Fe(p,2pn)^{54}Mn are shown in two groups in order to view overlaping experimental data. The top group was scaled upward by a factor of 10. The experimental data are from Brodzinski et al.,[28] Rayudu,[29,30] Schiekel et al.,[32] Schoen et al.,[36] Aleksandrov et al.,[27] Michel et al.,[37] Lavrukhina et al.,[34] Orth et al.[35] and Honda and Lal.[38]

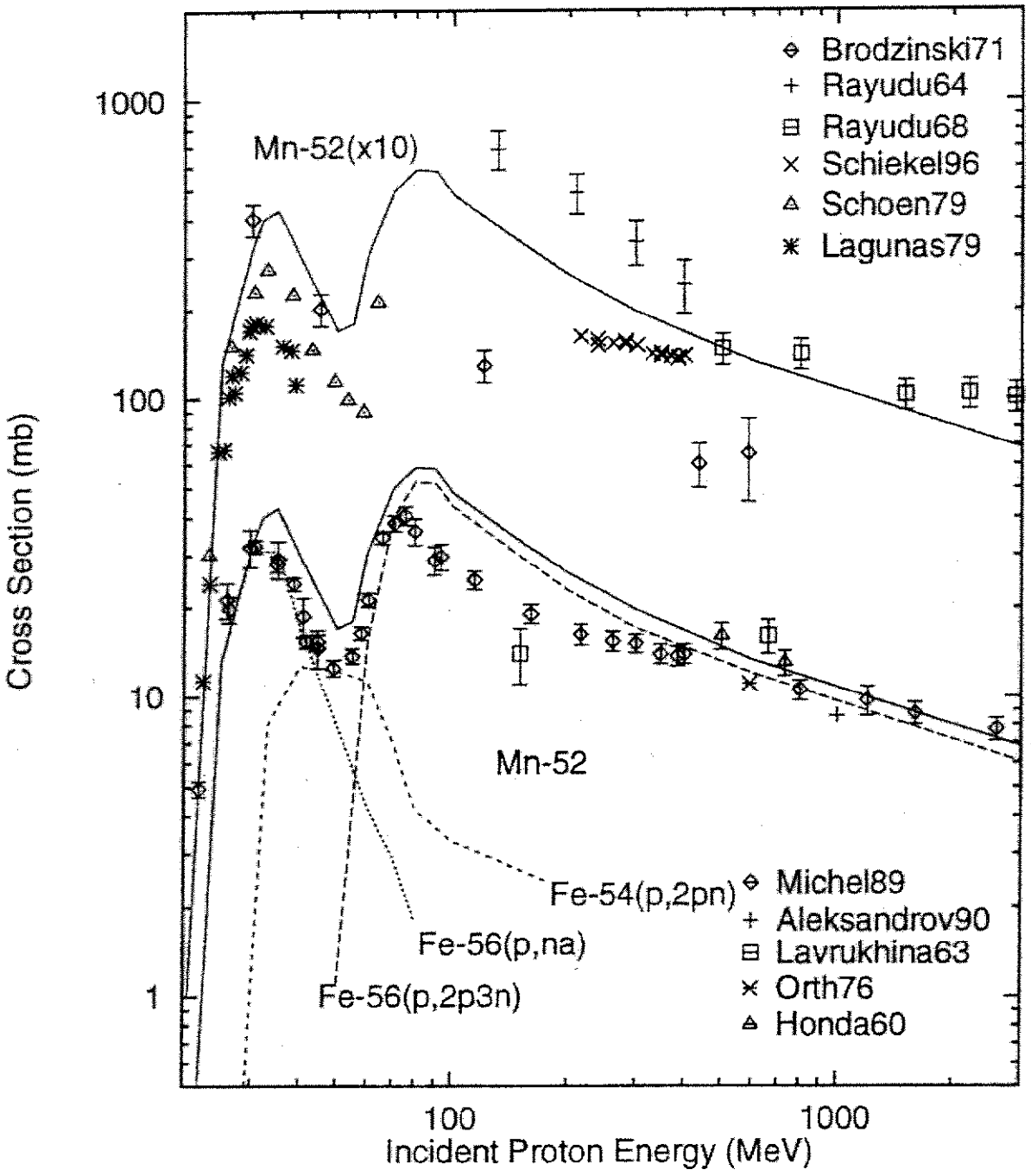

Fig. 5. Cross sections Fe(p,x)^{52}Mn are shown in two groups in order to view overlaping experimental data. The top group was scaled upward by a factor of 10. The low-energy peak is due to the ^{56}Fe(p,nα) reaction and the high-energy peak is from ^{56}Fe(p,2p3n). The ^{54}Fe(p,2pn) cross section fills the valley between the two peaks. The experimental data shown are from Brodzinski et al.,[28] Rayudu,[29,30] Schiekel et al.,[32] Schoen et al.,[36] Lagunas-Solar and Jungerman,[33] Michel et al.,[26] Aleksandrov et al.,[27] Lavrukhina et al.,[34] Orth et al.[35] and Honda and Lal.[39]

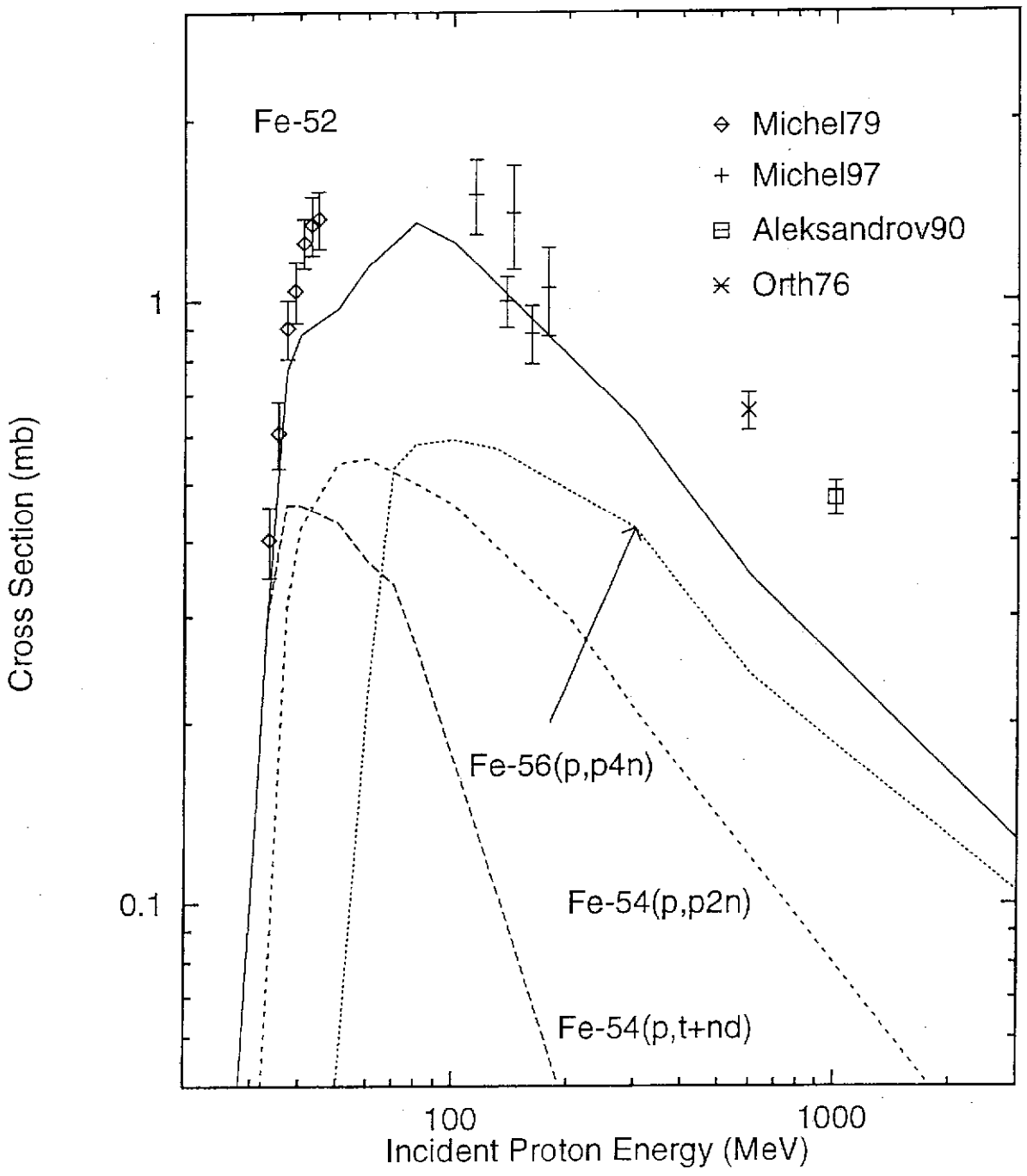

Fig. 6. Cross sections Fe(p,x)^{52}Fe. The calculated cross sections are sums of three components: ^{54}Fe(p,t+nd), ^{54}Fe(p,p2n) and ^{56}Fe(p,p4n). The measured data shown are from Michel et al.,[37,40] Aleksandrov et al.[27] and Orth et al.[35]

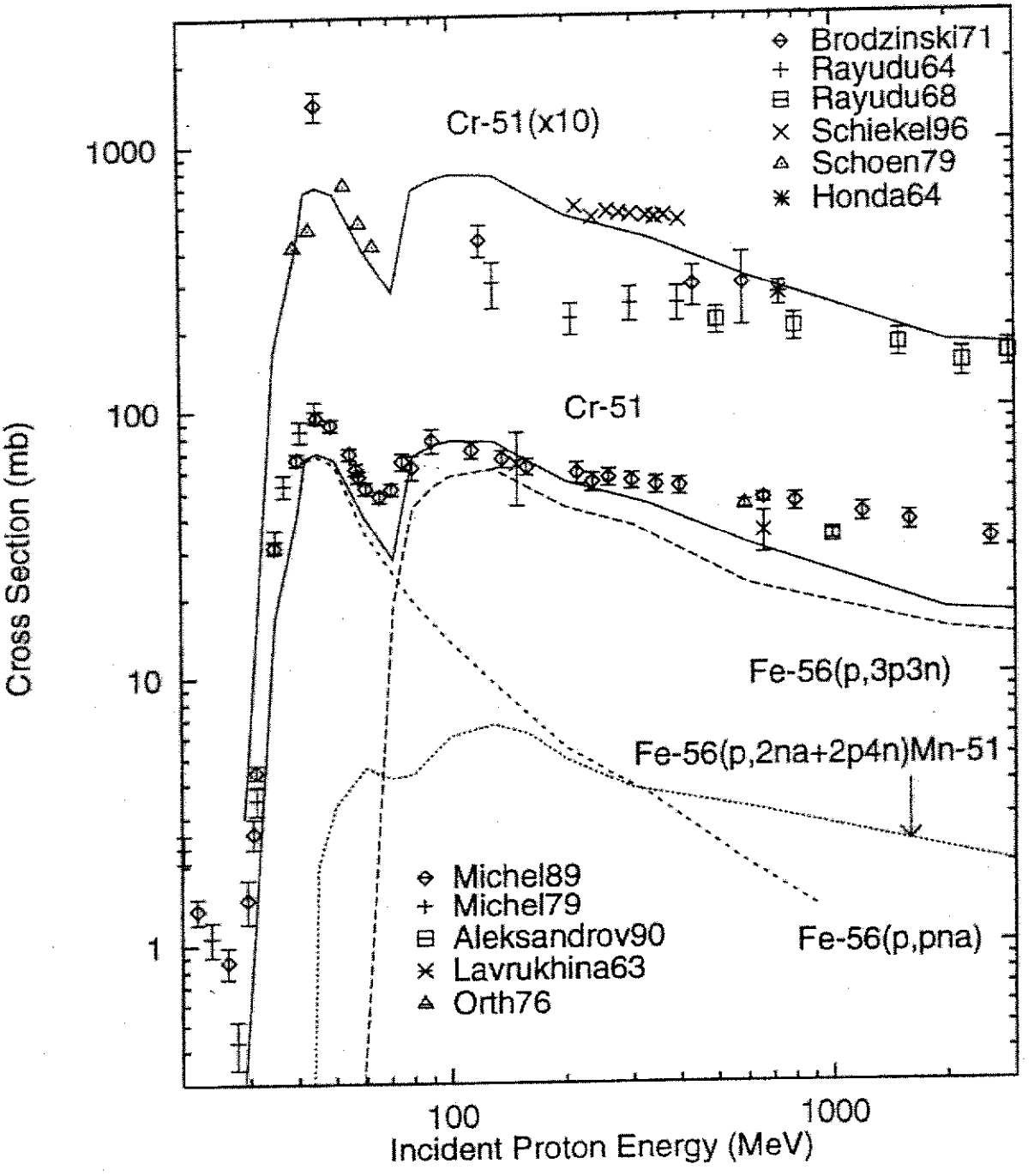

Fig. 7. Cross sections Fe(p,x)^{51}Cr are shown in two groups in order to view overlaping experimental data. The top group was scaled upward by a factor of 10. The low-energy peak is due to the ^{56}Fe(p,pnα) reaction and the high-energy peak is from ^{56}Fe(p,3p3n). The small component is from positron decays of ^{51}Mn via the ^{56}Fe(p,2nα+2p4n) reactions. The experimental data are from Brodzinski et al.,[28] Rayudu,[29,30] Schiekel et al.,[32] Schoen et al.,[36] Honda and Lal,[38] Michel et al.,[26,37] Aleksandrov et al.,[27] Lavrukhina et al.[34] and Orth et al.[35]

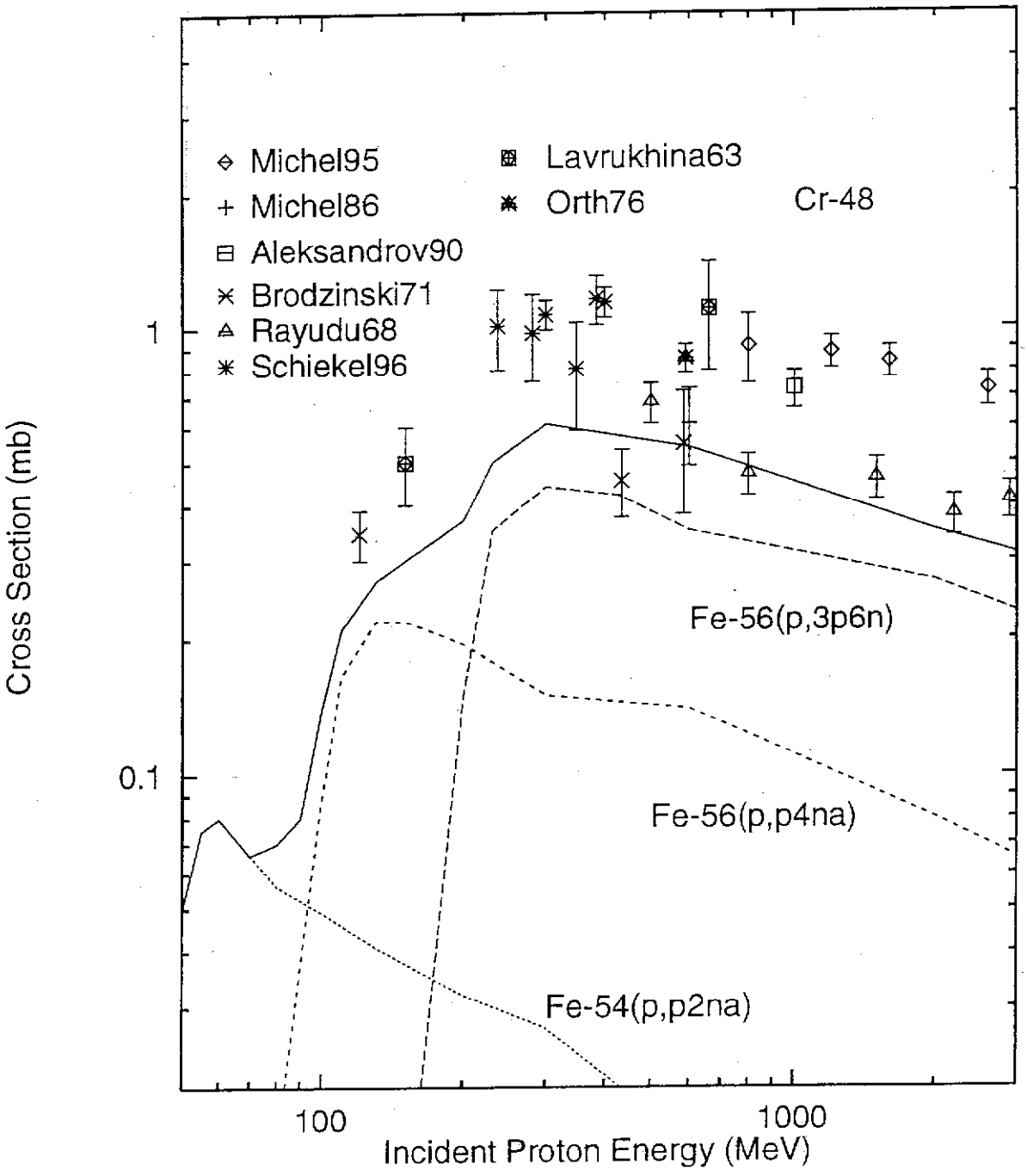

Fig. 8. Cross sections Fe(p,x)^{48}Cr. The calculated results are sums of three components: ^{54}Fe(p,p2nα), ^{56}Fe(p,p4nα) and ^{56}Fe(p,3p6n). The data shown are from Michel et al.,[10,41] Aleksandrov et al.,[27] Brodzinski et al.,[28] Rayudu,[30] Schiekel et al.,[32] Lavrukhina et al.[34] and Orth et al.[35]

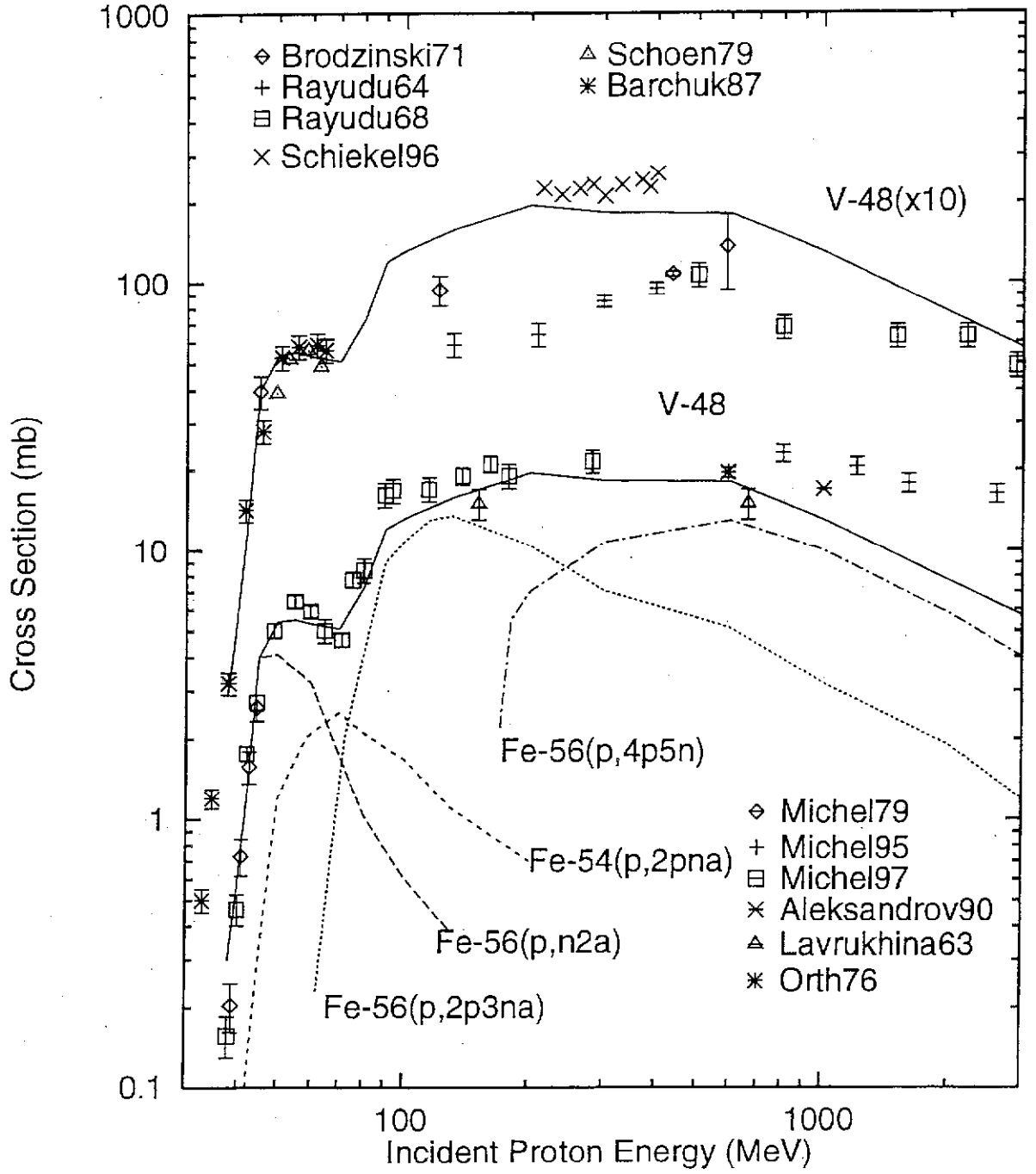

Fig. 9. Cross sections Fe(p,x)^{48}V. The two calculated components ^{56}Fe(p,n2α) and ^{54}Fe(p,2pnα) jointly contribute to the 55-MeV peak seen in the experimental data. The calculated component ^{56}Fe(p,2p3nα) contributes to the sharp rise seen in the experimental data at 100 MeV. The fourth component ^{56}Fe(p,4p5n) is important at high incident energies. The experimental data are from Brodzinski et al.,[28] Rayudu,[29,30] Schiekel et al.,[32] Schoen et al.,[36] Barchuk et al.,[42] Michel et al.,[37,10] Aleksandrov et al.,[27] Lavrukhina et al.[34] and Orth et al.[35]

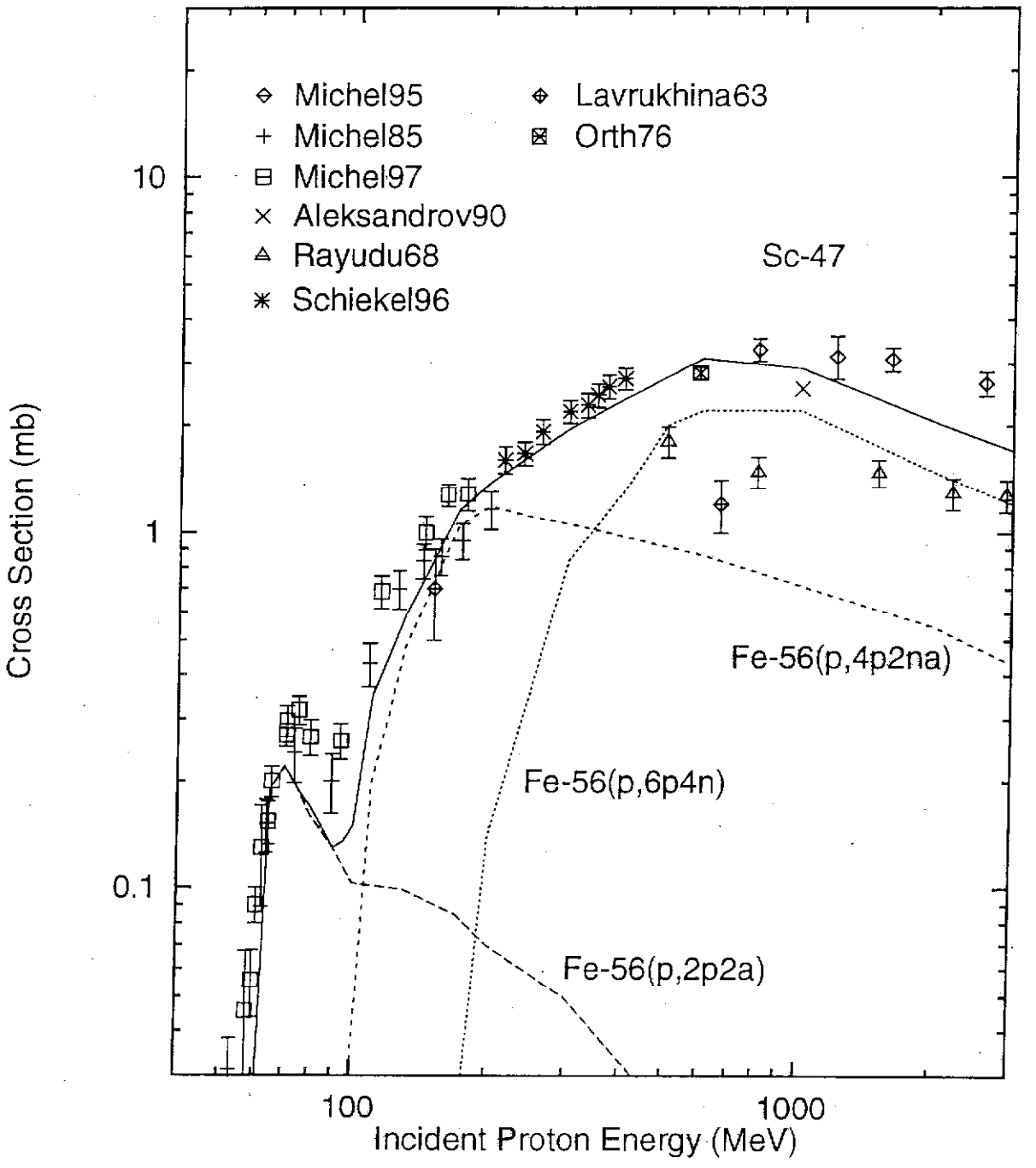

Fig. 10. Cross sections Fe(p,x)^{47}Sc. The calculated results are sums of three components: ^{56}Fe(p,2p2α), ^{56}Fe(p,4p2nα) and ^{56}Fe(p,6p4n). The experimental data are from Michel et al.,[10,43,40] Aleksandrov et al.,[27] Rayudu,[30] Schiekel et al.,[32] Lavrukhina et al.[34] and Orth et al.[35]

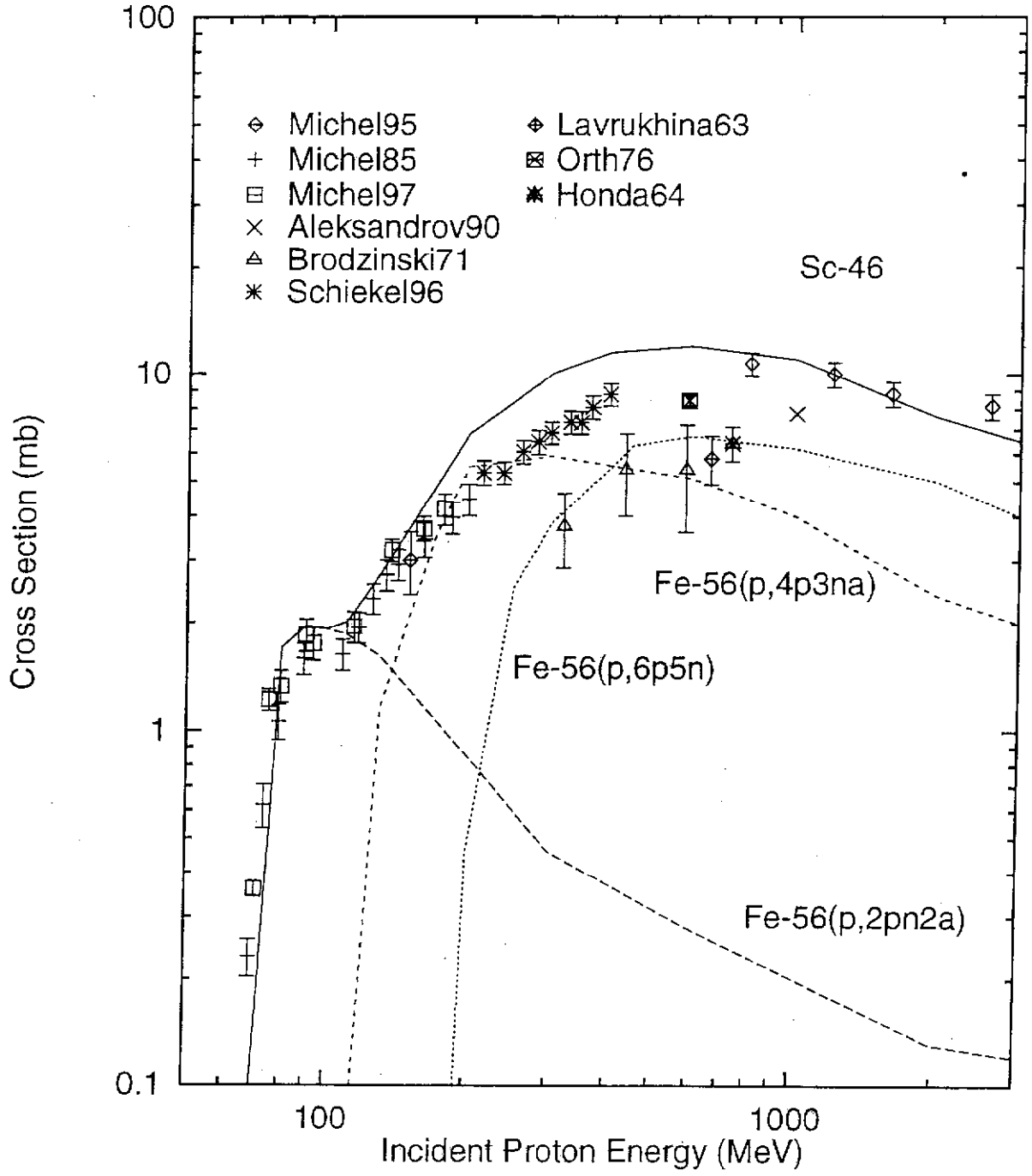

Fig. 11. Cross sections Fe(p,x)^{46}Sc. The calculated results are sums of three components: ^{56}Fe(p,2pn2α), ^{56}Fe(p,4p3nα) and ^{56}Fe(p,6p5n). The experimental data are from Michel et al.,[10,43,40] Aleksandrov et al.,[27] Brodzinski et al.,[28] Schiekel et al.,[32] Lavrukhina et al.,[34] Orth et al.[35] and Honda and Lal.[38]

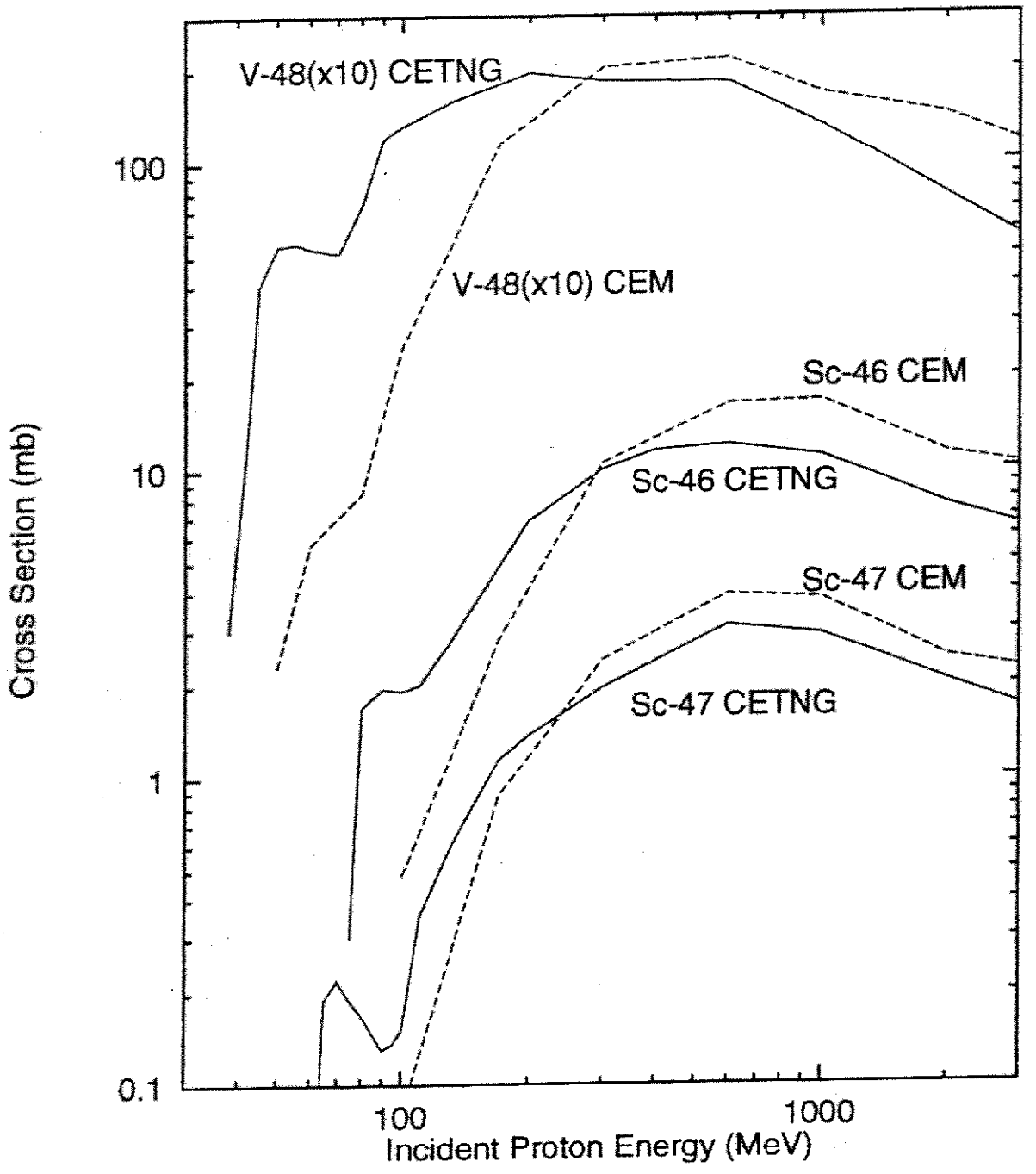

Fig. 12. Comparisons of the calculated Fe(p,x)^{48}V, ^{46}Sc and ^{47}Sc cross sections using CETNG with those using CEM. The cross sections calculated using CETNG are compared with experimental data in Figs. 9, 10 and 11, respectively. Those calculated with CEM are nearly identical to those calculated by Mashnik et al.[9] using CEM95.

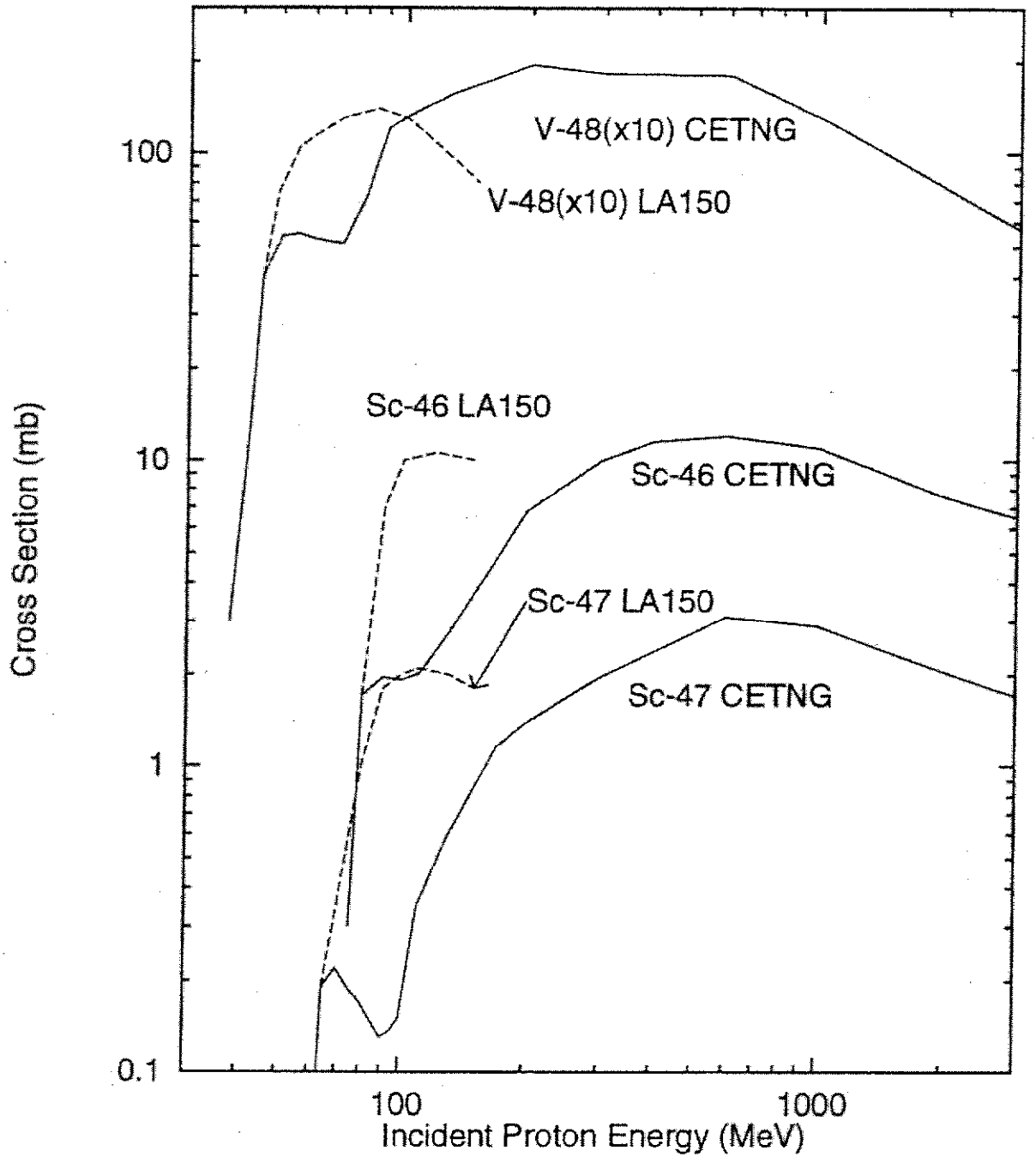

Fig. 13. Comparisons of the Fe(p,x)^{48}V, ^{46}Sc and ^{47}Sc cross sections calculated using CETNG with those calculated by Chadwick et al.[3] using GNASH (Ref. 44) and adopted for the LA150 data library. The cross sections calculated using CETNG are compared with experimental data in Figs. 9, 10 and 11, respectively, and are compared with those using CEM in Fig. 12.